

Supporting Information

Multiphase PdCu nanoparticles with improved C1 selectivity in ethanol oxidation

Wenxia Xu,^a Xueke Wu,^a Yueyue Yuan,^a Yingnan Qin,^a Yanru Liu,^a Zuochao Wang,^a Dan Zhang,^b
Hongdong Li,^a Jianping Lai^{*,a} and Lei Wang^{*,a,b}

^aKey Laboratory of Eco-chemical Engineering, Ministry of Education, Taishan scholar advantage and characteristic discipline team of Ecochemical progress and technology, Laboratory of Inorganic Synthesis and Applied Chemistry, College of Chemistry and Molecular Engineering, Qingdao University of Science and Technology, Qingdao 266042, P. R. China.

^bShandong Engineering Research Center for Marine Environment Corrosion and Safety Protection, College of Environment and Safety Engineering, Qingdao University of Science and Technology, Qingdao 266042, P. R. China.

Correspondence and requests for materials should be addressed to J.L. (e-mail: jplai@qust.edu.cn) and L.W. (e-mail: inorchemwl@126.com).

Contents

Experimental section.....	1
Figure S1.....	4
Figure S2.....	4
Figure S3.....	5
Figure S4.....	5
Figure S5.....	6
Figure S6.....	6
Figure S7.....	7
Figure S8.....	7
Figure S9.....	8
Figure S10.....	8
Figure S11.....	9
Figure S12.....	9
Figure S13.....	10
Figure S14.....	10
Figure S15.....	11
Figure S16.....	11
Figure S17.....	12
Figure S18.....	12
Table S1.....	13
Table S2.....	13
Table S3.....	15
Reference.....	16

Experimental Section

Materials. Sodium tetrachloropalladate ($\text{Cl}_4\text{Na}_2\text{Pd}$, 98%) was purchased from MACKLIN. Copper (II) acetyl acetonate ($\text{Cu}(\text{acac})_2$, 99%) was purchased from Energy Chemical. Ribose ($\text{C}_5\text{H}_{10}\text{O}_5$, 99%) was purchased from aladin. Oleylamine ($\text{C}_{18}\text{H}_{37}\text{N}$, 70%) was purchased from ALDRICH. 1-Octadecene ($\text{C}_{18}\text{H}_{36}$, 90%), Multi-walled carbon nanotubes (MWCNT) was purchased from Shenzhen Hongdachang Evolution Technology Co., Ltd. Sulfuric acid (H_2SO_4 , 95–98%) and nitric acid (HNO_3 , 95–98%) was purchased from HUSHI.

Preparation of carboxylated carbon nanotubes. First, 50.0 mg of carbon nanotubes (CNT) powder was added into the mixed solution of concentrated HNO_3 and concentrated H_2SO_4 (volume ratio 1:3), ultrasound at room temperature for 1-2 h, and filtered. Second, the samples were exposed to 1.0 M HCl for 30 min and filtered. Finally, wash with deionized water, dry, multi-walled carbon nanotubes (MWCNT) were obtained.

Preparation of PdCu nanoparticle. First, 9.8 mg of NaPdCl_4 , 13.3 mg of $\text{Cu}(\text{acac})_2$, 15 mg of Ribose, 2.5 mL of Oleamine and 2.5 mL of 1-Octadecene were added into the pressure-resistant vials, the ultrasonic time was 0.5 h. Then it was heated in an oil bath at 180 °C for 3 h. Cooling to room temperature and centrifuging to collect the product. The product was washed 3 times in the mixed solution of methanol: ethanol = 1:2 and dried to obtain PdCu powder. Add 5.0 mL cyclohexane, set aside.

Preparation of PdCu/CNT. 30.0 mg of MWCNT was added into isopropanol, ultrasound 2 h. 2.0 mL of already prepared PdCu solution, and cyclohexane was added to the solution, ultrasound 1 h. At the end of ultrasound, the two solutions were mixed and ultrasound was performed for 30 min. Ethanol washing and drying.

Preparation of PdCu/CNT-200, PdCu/CNT-300, PdCu/CNT-400, PdCu/CNT-500, PdCu/CNT-600. Taking dried PdCu/CNT powder and calcining it in tube furnace with Ar and H_2 (10%) mixture, calcining temperature is 200 °C, 300°C, 400 °C, 500 °C, 600 °C, respectively, the finished samples were named PdCu/CNT-200, PdCu/CNT-300, PdCu/CNT-400, PdCu/CNT-500, PdCu/CNT-600 respectively.

Characterization. For the characterization of the catalyst structure, powder X-ray diffraction (XRD) patterns were obtained by testing with an X'Pert-Pro MPD diffractometer at 40 KV and 40 mA $\text{Cu K}\alpha$ radiation. Scanning electron microscopy (SEM) patterns were obtained with a Hitachi S-4800 instrument. Transmission electron microscopy (TEM) and high-resolution TEM (HRTEM) were obtained with a FEI

Tecnai-G2 F30 instrument at a voltage of 300 KV. X-ray photoelectron spectra (XPS) were obtained using a monochromatic Al K_α source when the Axis Supra spectrometer was at 15 mA and 14 kV. The valence states of each element of the catalyst were analyzed using Casa XPS software, where all spectra were calibrated by C 1s spectroscopy and the standard value was set at 284.5 eV. The elemental content of the catalyst was determined by inductively coupled plasma atomic emission spectrometry (ICP-AES, Varian 710-ES) and used for a series of calculations. After stability testing by dropping the catalyst onto carbon paper, the catalyst was dried and scraped off for post-reaction SEM, TEM, XRD and XPS.

Electrochemical measurements. Preparation of 1 mg mL⁻¹ catalyst dispersion: Prepare 1.0 mL of isopropanol, add ultrapure water and 5% Nafion volumetric ratio, the volume ratio of the three isopropanol: ultrapure water: Nafion = 3: 1: 0.05, take 1.0 mg catalyst and add it to the mixture of the three and sonicate for 1 h.

Electrochemical testing: A three-electrode system was used, in which the working electrode was a glassy carbon electrode (GCE) with a diameter of 3 mm and an area of 0.07065 cm², the reference electrode was Ag/AgCl, and the counter electrode was a graphite rod electrode. The chemical workstation was a CHI 760E electrochemical workstation from Shanghai Huachen Instruments, China, for electrochemical testing. 10.0 μL of the prepared dispersion was taken, dropped on the surface of the working electrode, dried and then electrochemical tests were performed. The EOR properties of the catalysts were evaluated using cyclic voltammetry at a scan rate of 50 mV s⁻¹ tested in saturated solutions of 1.0 M KOH or 1.0 M KOH + 1.0 M CH₃CH₂OH. All potentials in this experiment were calibrated with a reversible hydrogen electrode, and all polarization curves were corrected for 95% iR. We also performed stability tests in a 1.0 M KOH solution using chronoamperometry. In addition, the stability of the catalyst was tested again by measuring the CV after 1000 cycles. At frequencies ranging from 0.1 Hz to 100 KHz, electrochemical impedance spectroscopy (EIS) measurements were performed in saturated 1.0 M KOH solution.

Electrochemical in Situ FTIR reflectance spectroscopy. Electrochemical in situ FTIR reflectance spectra were tested with a Nexus 870 spectrometer (Nicolet) equipped with a liquid nitrogen-cooled MCT-A detector (used to obtain electrochemical in situ Fourier transform infrared (FTIR) reflectance spectroscopy). In the test, infrared light sequentially passes through a window and a thin layer of solution to form a reflection at the surface of the electrode. At the same time the working electrode was coated with the prepared catalyst and inserted in a solution containing ethyl 1.0 M KOH + 1.0 M CH₃CH₂OH for the reaction. The obtained spectrum is expressed as the relative change in reflectance ($\Delta R/R$) using the following equation $\Delta R/R =$

$(R(ES) - R(ER)) / R(ER)$ is calculated. $R(ES)$ is the single-beam spectrum collected at the sample potential ES . $R(ER)$ is the single-beam spectrum collected at the reference potential ER . And ER was fixed at 0.1 V (vs. RHE).

Calculation of C1 selectivity: The yield of possible EOR product can be conducted by GC and Faraday formula. Firstly, a series of acetic acid and acetaldehyde standard solutions has been made with a stepped concentration (0.1-5 ppm). The standard curve can be drawn with the integral area of GC peak and the concentration of standard solution. Secondly, a long time i-t test has been conducted to collect the product to be measure. The concentration of as-produced acetic acid and acetaldehyde can be calculated by the standard curve. Finally, based on the Faraday formula, the Faradic efficiency of as-produced acetic acid and acetaldehyde can be calculated as follow:

$$FE = (N \times n \times 96485) / Q \times 100\%$$

N is the moles of products, n is the number of electron transfer, Q is the total amount of consumed charge during i-t test. The total FE of EOR was assumed as 100%, the possible C1 selectivity is the residue of C2 pathway.

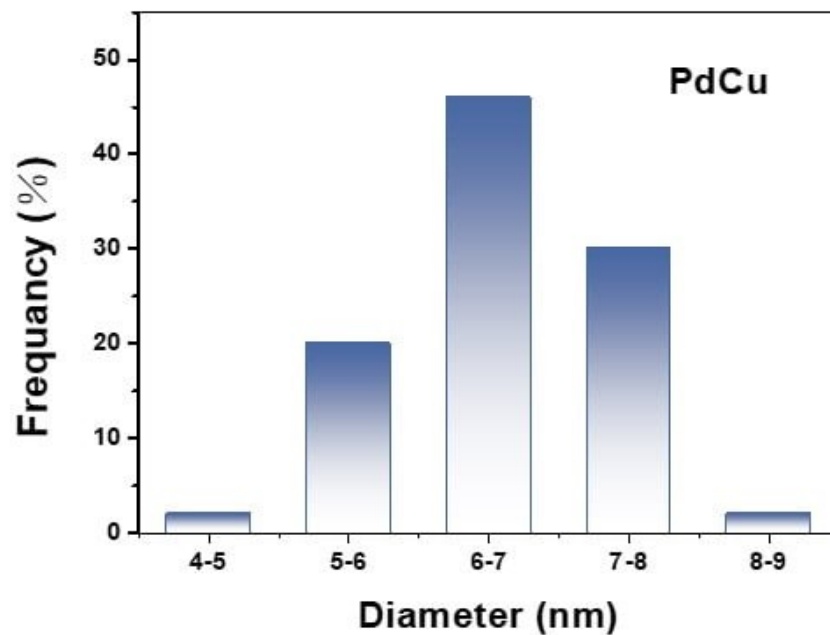


Figure S1. Particle size distribution of PdCu particles before loading.

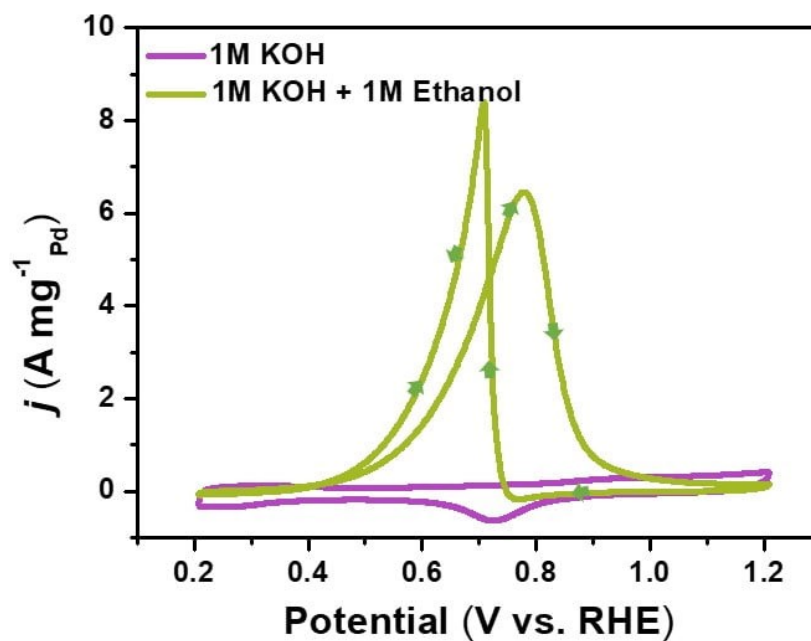


Figure S2. CV curves of the calcined PdCu/CNT for EOR in 1.0 M KOH and 1.0 M KOH + 1.0 M CH₃CH₂OH solution at a scan rate of 50 mV s⁻¹.

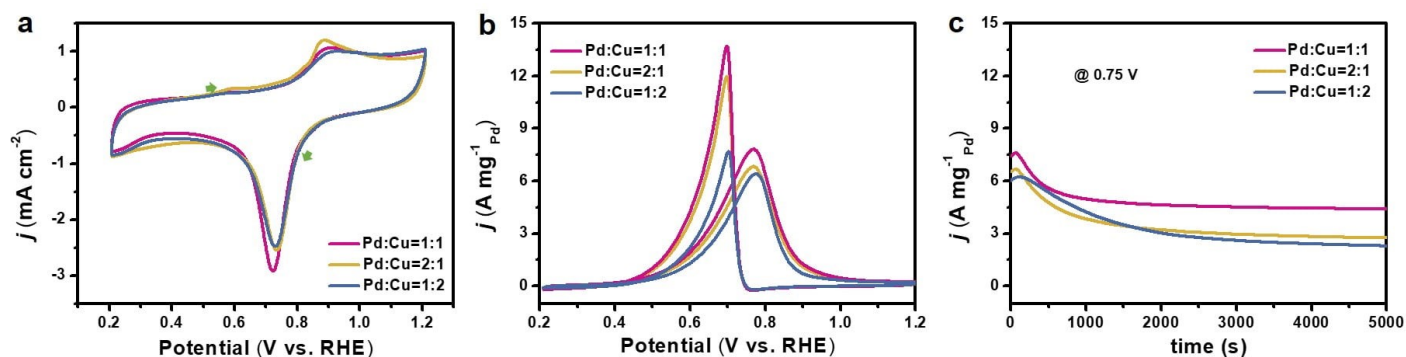


Figure S3. PdCu/CNT catalysts prepared under different Pd:Cu ratios of 1:2, 1:1 and 2:1. (a) CV curves in 1.0 M KOH. (b) CV curves for EOR in 1.0 M KOH + 1.0 M CH₃CH₂OH solution. (c) Chronoamperometric tests for EOR in 1.0 M KOH + 1.0 M CH₃CH₂OH solution at 0.75 V (vs. RHE).

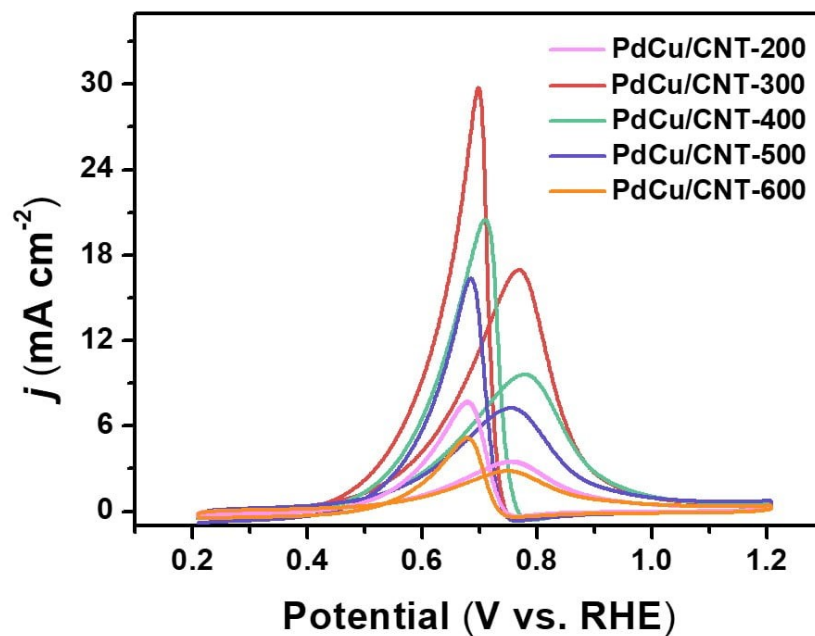


Figure S4. CV curves of PdCu/CNT calcined at 200 °C, 300 °C, 400 °C, 500 °C, 600 °C for EOR in 1.0 M KOH + 1.0 M CH₃CH₂OH solution at a scan rate of 50 mV s⁻¹.

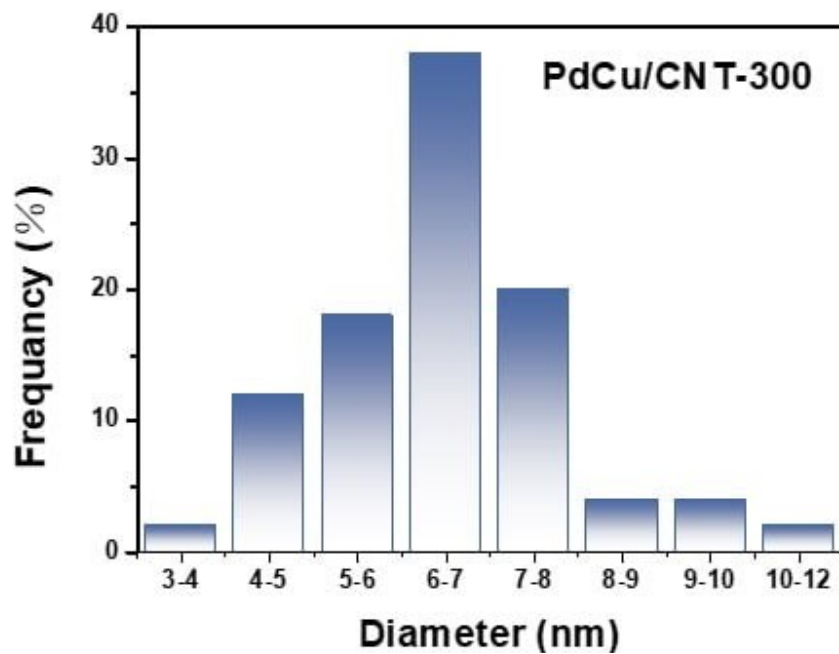


Figure S5. Particle size distribution of PdCu/CNT-300.

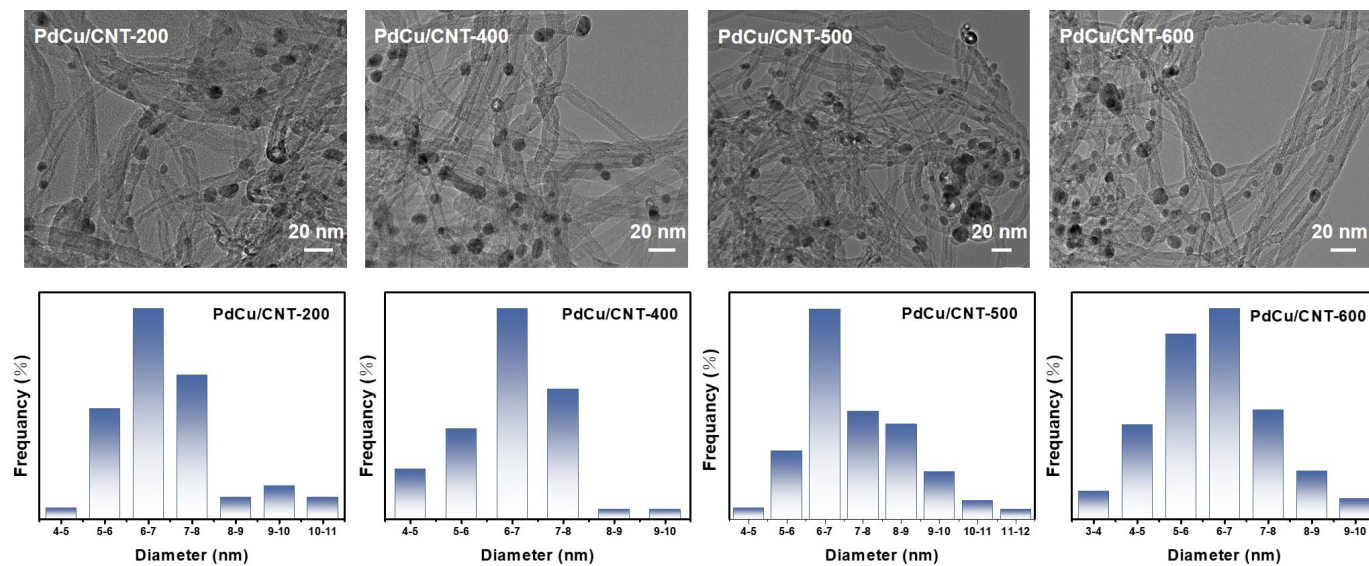


Figure S6. Particle size distribution of PdCu/CNT-200, PdCu/CNT-400, PdCu/CNT-500 and PdCu/CNT-600.

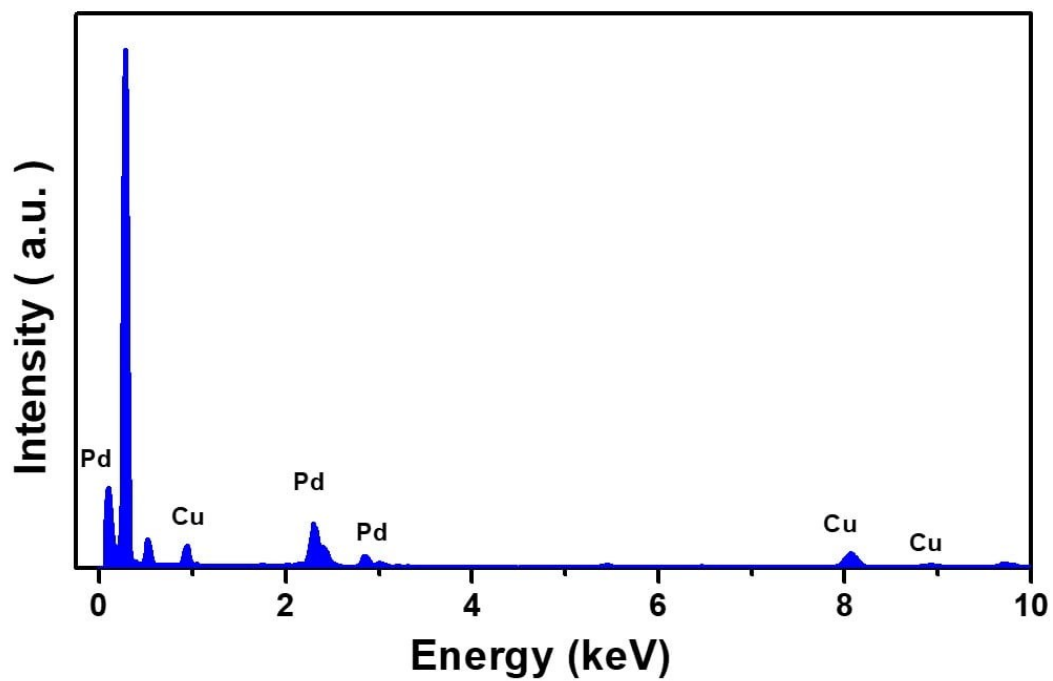


Figure S7. EDX spectrum of PdCu/CNT-300.

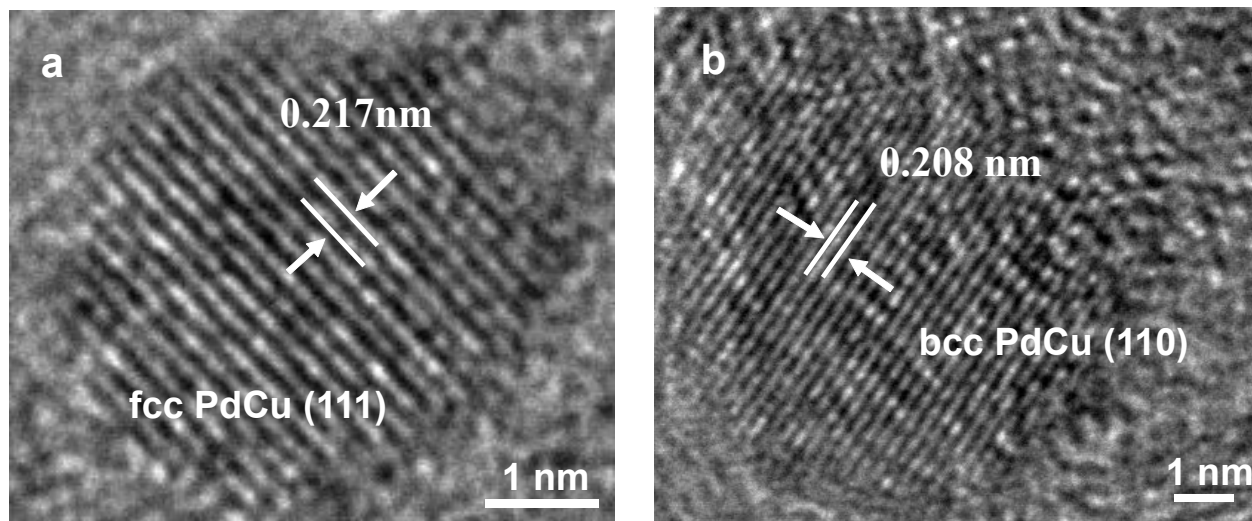


Figure S8. HRTEM images of (a) PdCu/CNT-200, (b) PdCu/CNT-600.

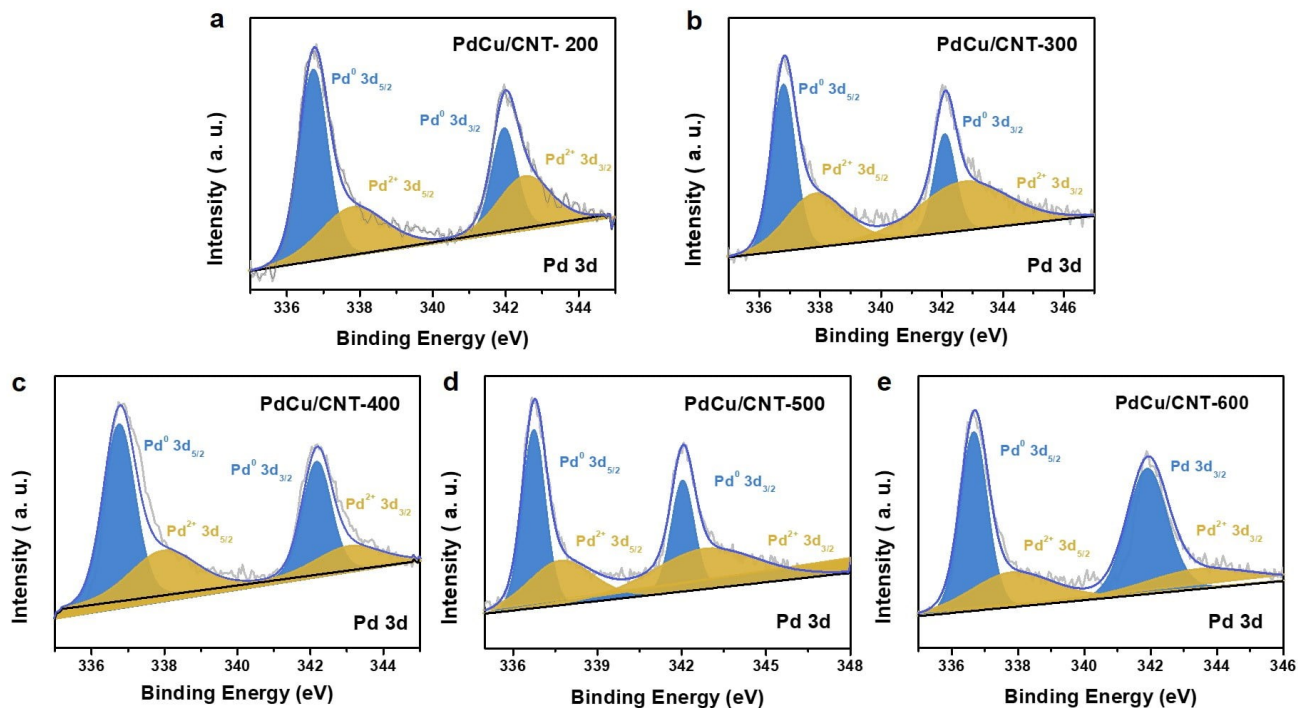


Figure S9. Pd 3d high-resolution XPS spectra of PdCu/CNT calcined at different temperatures.

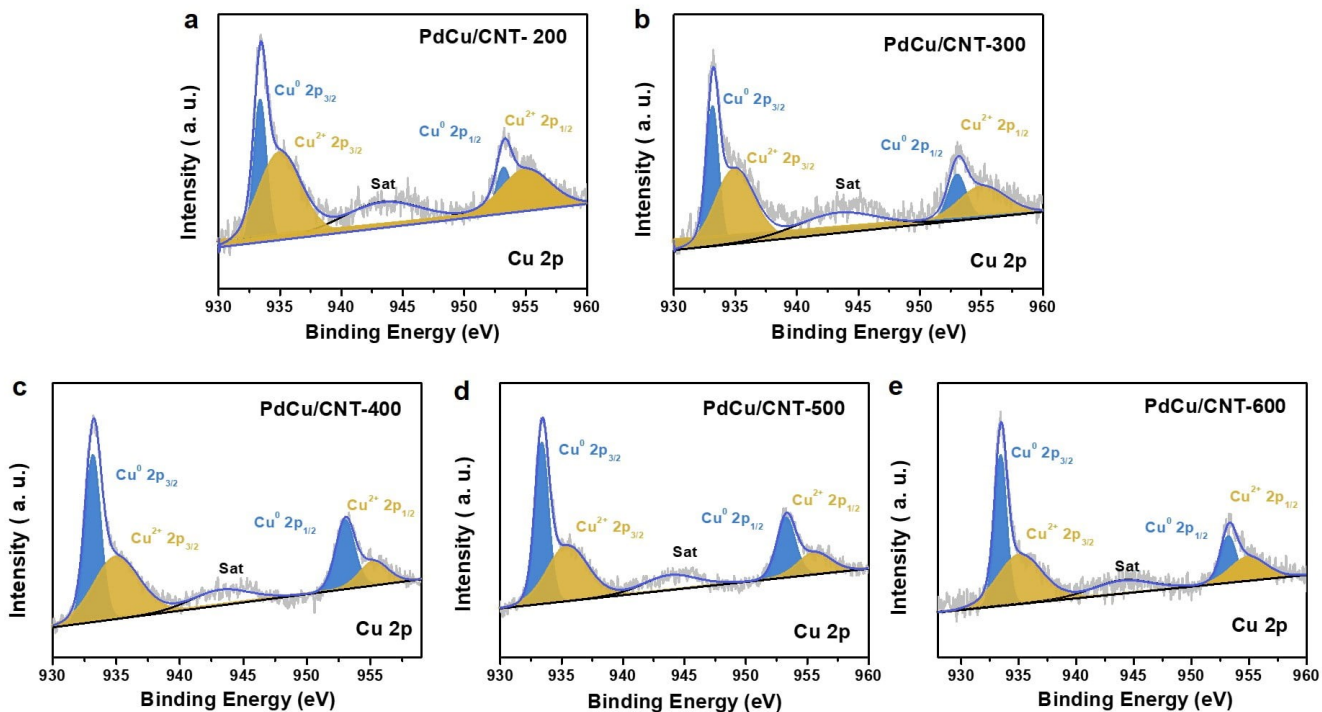


Figure S10. Cu 2p high-resolution XPS spectra of PdCu/CNT calcined at different temperatures.

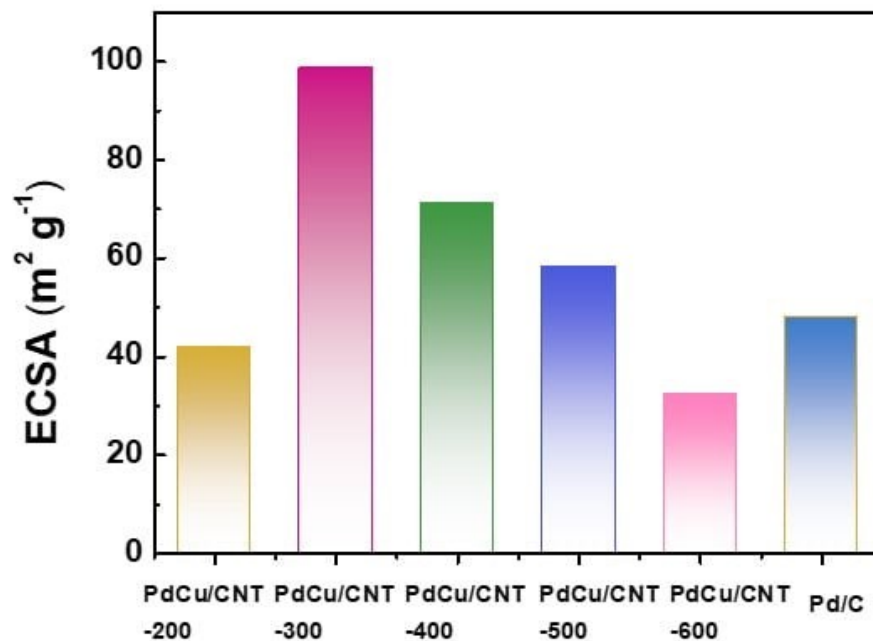


Figure S11. ECSA values of PdCu/CNT-200, PdCu/CNT-300, PdCu/CNT-400, PdCu/CNT-500, PdCu/CNT-600 and Pd/C in 1.0 M KOH aqueous solution.

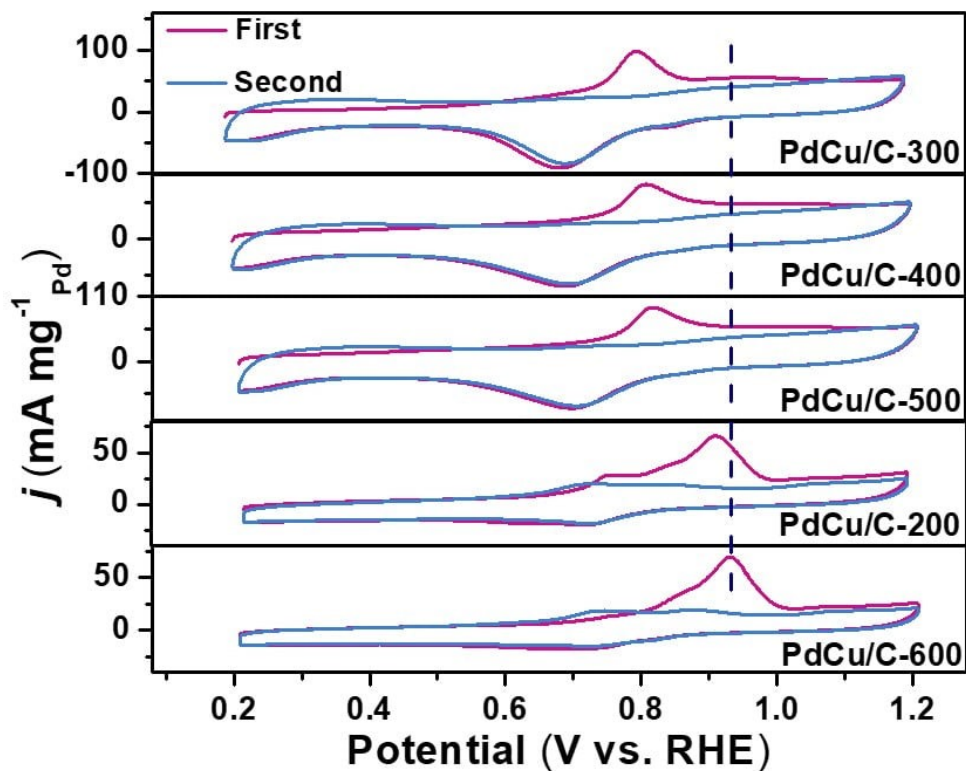


Figure S12. CO stripping curves of PdCu/CNT-200, PdCu/CNT-300, PdCu/CNT-400, PdCu/CNT-500 and PdCu/CNT-600 catalys.

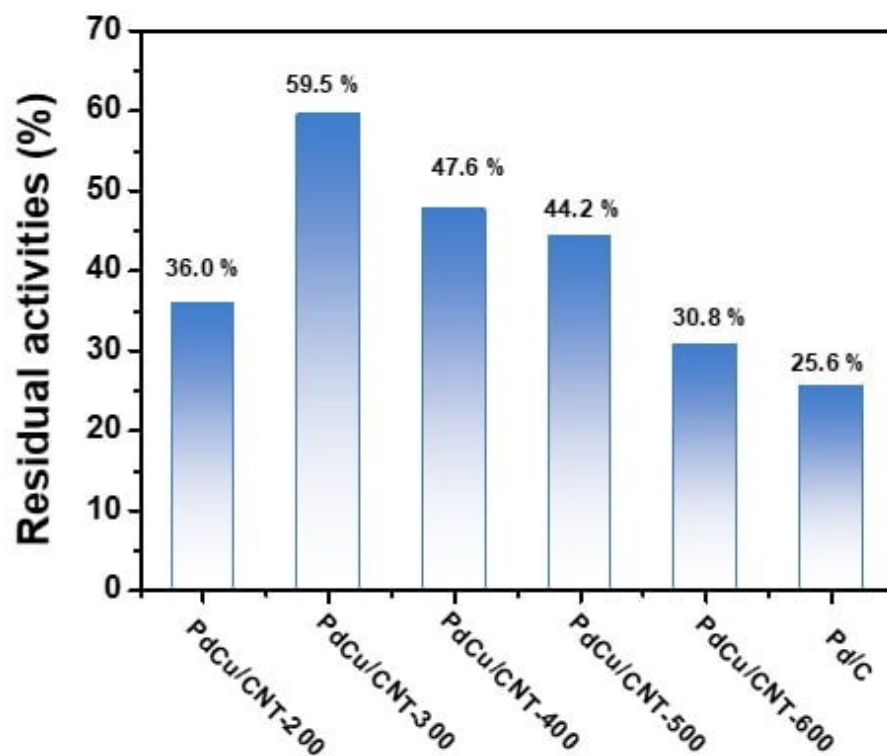


Figure S13. Histograms of residual mass activities for the catalysts.

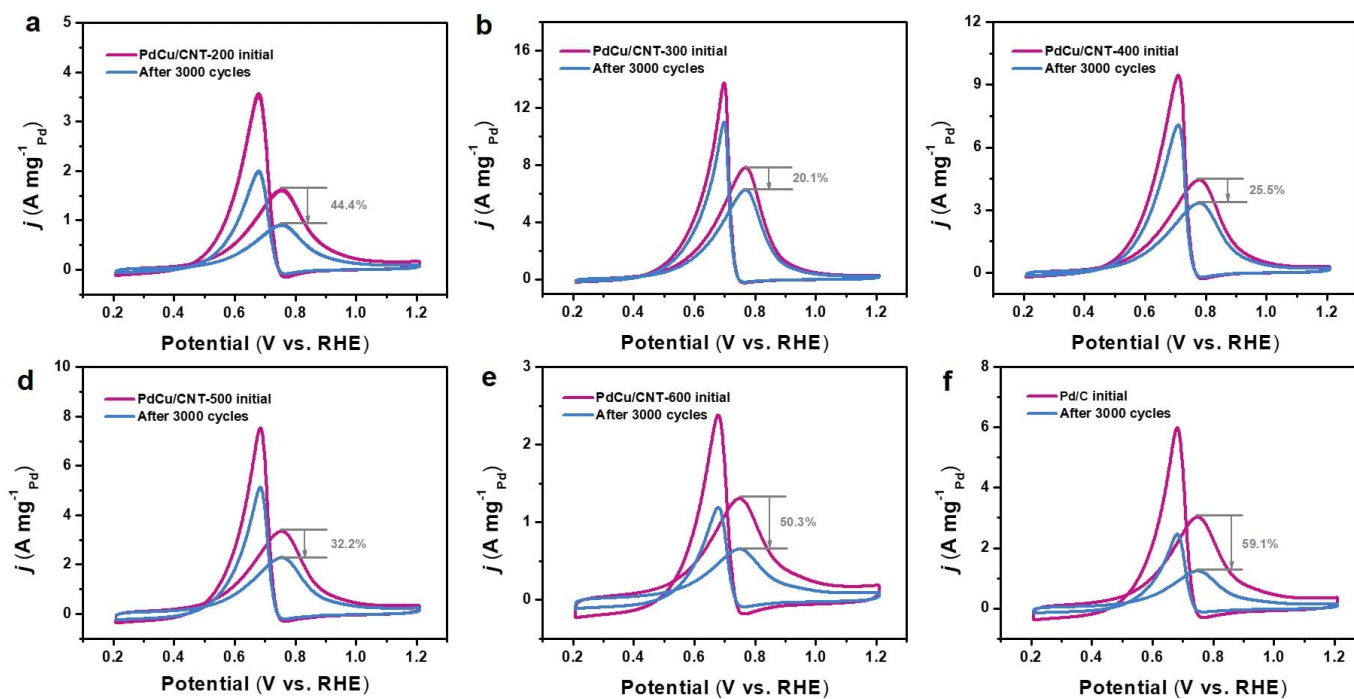


Figure S14. Cycle stability of (a) PdCu/CNT-200, (b) PdCu/CNT-300, (c) PdCu/CNT-400, (d) PdCu/CNT-500, (e) PdCu/CNT-600 and Pd/C recorded in 1.0 M KOH + 1.0 M CH₃CH₂OH solution after 3000 cycles.

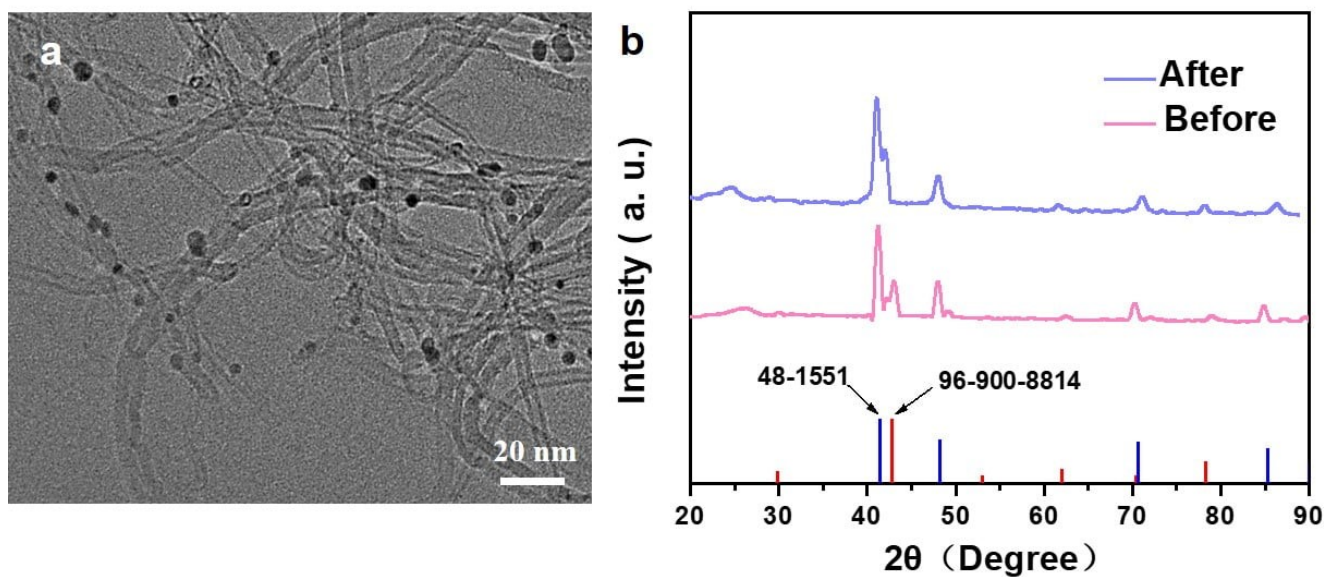


Figure S15. Comparison of morphology and electronic structure of PdCu/CNT-300 catalyst before and after EOR stability test. (a) TEM image after the EOR stability test. (b) XRD pattern before and after the EOR stability test.

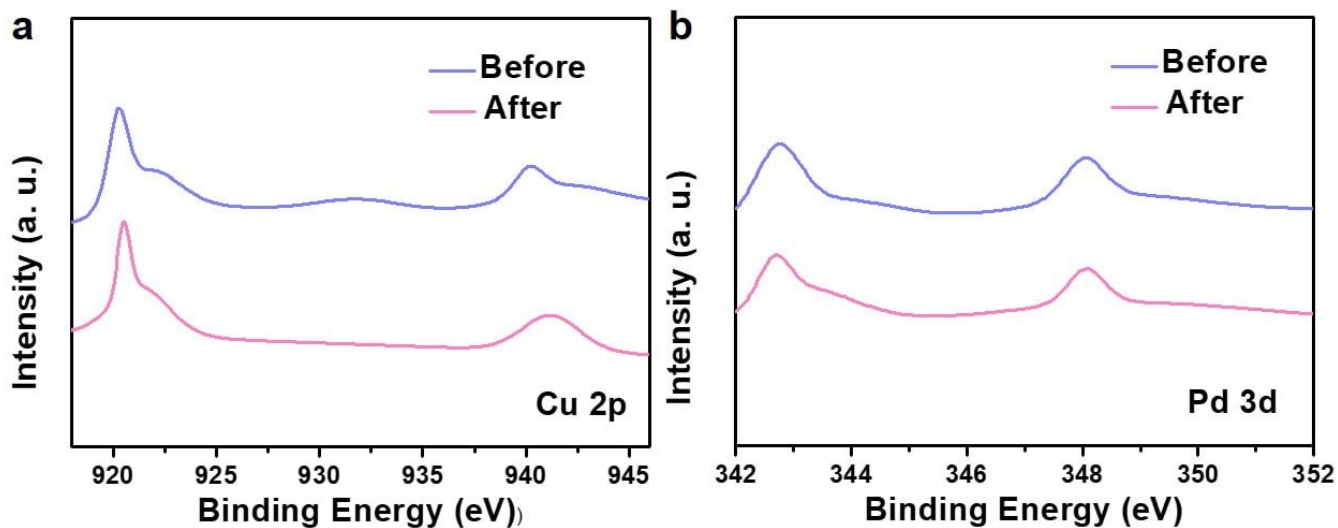


Figure S16. XPS diagram before and after reaction of (a) Cu 2p, (b) Pd 3d and (c) C 1s.

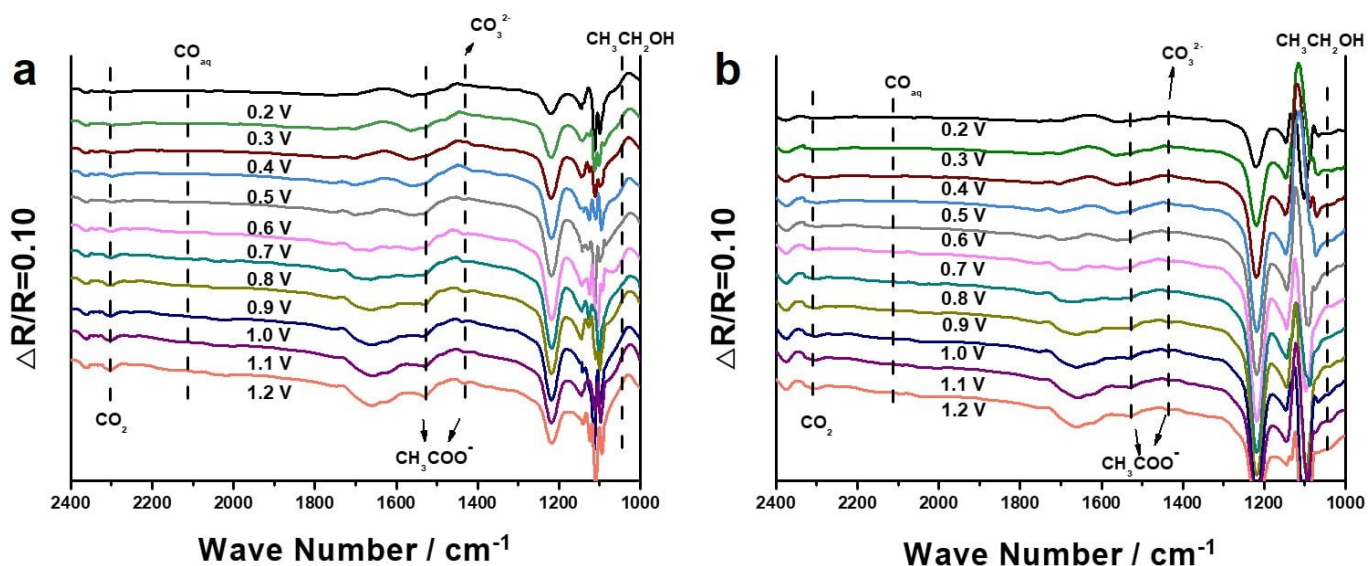


Figure S17. In situ Fourier transform spectra of (a) PdCu/CNT-200 and (b) Pd/C of EOR occur at the interval of 0.10 V (vs.RHE).

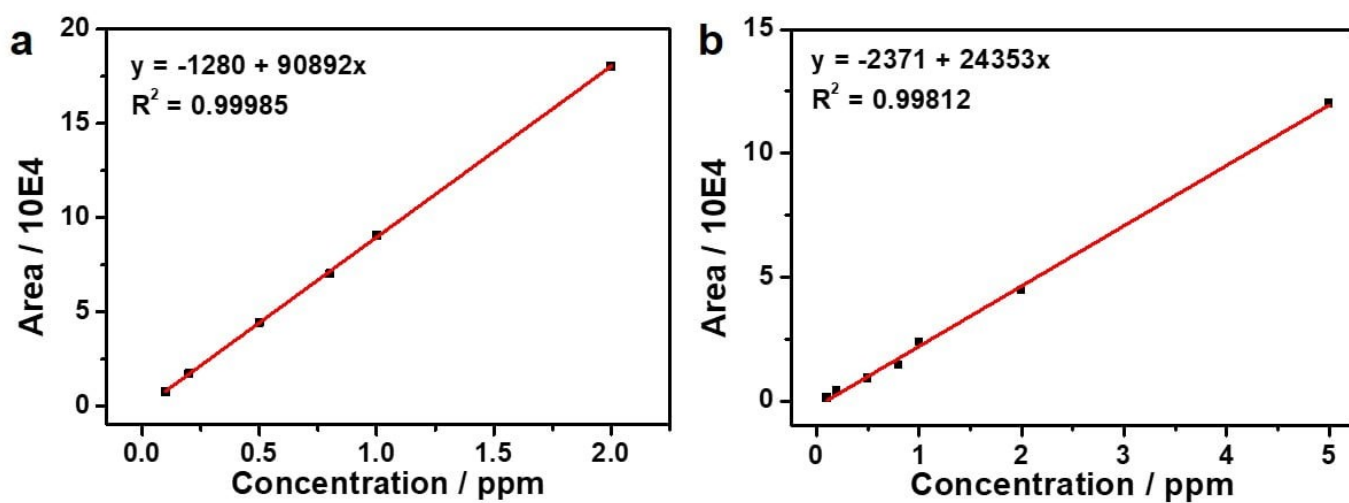


Figure S18. Standard curves of a) acetate and b) acetaldehyde in GC.

Table S1. Mass ratio of prepared catalysts conducted by ICP-AES

Pd:Cu ratios in precursors	Pd:Cu tested by ICP-AES
1:2	0.661:1
1:1	1.164:1
2:1	1.741:1

Table S2. Recently, some typical electrocatalysts containing Pd for EOR in alkaline conditions have been reported.

Catalysts	Electrolyte	Mass Activity (A mg⁻¹)	Specific Activity (mA cm⁻²)	Ref.
PdCu/C-300	1.0 M KOH + 1.0 M Ethanol	7.8	17.0	This work
TS-Pd/C	1.0 M KOH + 1.0 M Ethanol	1.84	3.22	1
Pd NPs	1.0 M KOH + 1.0 M Ethanol	1.02	2.5	2
Pd/NCB@NGS-2	1.0 M KOH + 1.0 M Ethanol	2.7	-	3
ultrathin Pd nanomeshes	1.0 M KOH + 1.0 M Ethanol	5.40	7.09	4
Pd ₅₀ Ag ₅₀	1.0 M KOH + 1.0 M Ethanol	1.97	6	5

Pt-Pd/RGO	1.0 M KOH + 1.0 M Ethanol	1.48	0.8	6
Pd@CoP NSs/CFC	1.0 M KOH + 1.0 M Ethanol	1.41	3.5	7
PdP ₂ /rGO	0.5 M KOH + 0.5 M Ethanol	1.60	1.5	8
Pt _{1-x} Pd _x /C	1.0 M KOH + 1.0 M Ethanol	2.6	–	9
Pd/GS	0.1 M NaOH + 0.4 M Ethanol	1.8	–	10
Pd ₅₂ -Ni ₄₈ /NS/CA	1.0 M NaOH + 0.5 M Ethanol	2.96	–	11
Pd/NiSA	1.0 M KOH + 1.0 M Ethanol	1.2	–	12
Pd/C	1.0 M KOH + 1.0 M Ethanol	1.05	–	13
Au@Pd NRs	1.0 M KOH + 1.0 M Ethanol	2.92	–	14
Pd/Cu ₃ P/RGO	1.0 M KOH + 1.0 M Ethanol	1.55	–	15
PdS _x /C	1.0 M KOH + 1.0 M Ethanol	0.16	–	16
PdCu ₂	1.0 M KOH + 1.0 M Ethanol	1.6	2.5	17

Table S3. Recently, some of the reported Pd-based catalysts for the selective C1 pathway of ethanol oxidation in alkaline solutions.

Catalysts	Faradaic Efficiency of the C1	Ref.
PdCu/C-300	53.9%	This work
Pd-Ni (OH) ₂ /GO	24%	13
CoP/RGO-Pd	27.6%	18
Pd-Au HNS/C	33.2%	19
Pd/CuO-Ni(OH) ₂ /C	22.5%	20
Ag@Pd ₂ P _{0.2}	19%	21
Pd/C	3.2%	22

Reference

1. C. Liu, Y. Shen, J. Zhang, G. Li, X. Zheng, X. Han, L. Xu, S. Zhu, Y. Chen, Y. Deng and W. Hu, Multiple twin boundary-regulated metastable Pd for ethanol oxidation reaction, *Adv. Energy Mater.*, 2022, **12**, 2103505.
2. H. Xu, H. Shang, C. Wang, L. Jin, C. Chen and Y. Du, Nanoscale engineering of porous Fe-doped Pd nanosheet assemblies for efficient methanol and ethanol electrocatalyses, *Nanoscale* 2020, **12**, 2126-2132.
3. S. Li, J. Shu, S. Ma, H. Yang, J. Jin, X. Zhang and R. Jin, Engineering three-dimensional nitrogen-doped carbon black embedding nitrogen-doped graphene anchoring ultrafine surface-clean Pd nanoparticles as efficient ethanol oxidation electrocatalyst, *Appl. Catal. B Environ.*, 2021, **280**, 119464.
4. J. Ge, P. Wei, G. Wu, Y. Liu, T. Yuan, Z. Li, Y. Qu, Y. Wu, H. Li, Z. Zhuang, X. Hong and Y. Li, Ultrathin palladium nanomesh for electrocatalysis, *Angew. Chem. Int. Ed.*, 2018, **57**, 3435-3438.
5. S. Fu, C. Zhu, D. Du and Y. Lin, Facile one-step synthesis of three-dimensional Pd–Ag bimetallic alloy networks and their electrocatalytic activity toward ethanol oxidation, *ACS Appl. Mater. Interfaces*, 2015, **7**, 13842-13848.
6. F. Ren, H. Wang, C. Zhai, M. Zhu, R. Yue, Y. Du, P. Yang, J. Xu and W. Lu, Clean method for the synthesis of reduced graphene oxide-supported PtPd alloys with high electrocatalytic activity for ethanol oxidation in alkaline medium, *ACS Appl. Mater. Interfaces*, 2014, **6**, 3607-3614.
7. S.-H. Ye, J.-X. Feng and G.-R. Li, Pd nanoparticle/CoP nanosheet hybrids: highly electroactive and durable catalysts for ethanol electrooxidation, *ACS Catal.*, 2016, **6**, 7962-7969.
8. J. Liu, Z. Luo, J. Li, X. Yu, J. Llorca, D. Nasios, J. Arbiol, M. Meyns and A. Cabot, Graphene-supported palladium phosphide PdP₂ nanocrystals for ethanol electrooxidation, *Appl. Catal. B Environ.*, 2019, **242**, 258-266.
9. Q. Zhang, T. Chen, R. Jiang and F. Jiang, Comparison of electrocatalytic activity of Pt_{1-x}Pd_x/C catalysts for ethanol electro-oxidation in acidic and alkaline media, *RSC Adv.*, 2020, **10**, 10134-10143.
10. R. Venkata Jagadeesh and V. Lakshminarayanan, Enhanced electrocatalytic activity of Pd and Pd-polyaniline nanoparticles on electrochemically exfoliated graphite sheets, *Appl. Catal. B Environ.*, 2019, **251**, 25-36.
11. T. Raj kumar, G. Gnana kumar and A. Manthiram, Biomass-derived 3D carbon aerogel with carbon shell-confined binary metallic nanoparticles in CNTs as an efficient electrocatalyst for microfluidic direct ethylene glycol fuel cells, *Adv. Energy Mater.*, 2019, **9**, 1803238.
12. T. Nitaya, Y. Cheng, S. Lu, K. Poochinda, K. Pruksathorn and S. P. Jiang, Unusual synergetic effect of nickel single atoms on the electrocatalytic activity of palladium for alcohol oxidation reactions in alkaline media, *Chem. Commun.*, 2018, **54**, 12404-12407.
13. W. Huang, X.-Y. Ma, H. Wang, R. Feng, J. Zhou, P. N. Duchesne, P. Zhang, F. Chen, N. Han, F. Zhao, J. Zhou, W.-B. Cai and Y. Li, Promoting effect of Ni(OH)₂ on palladium nanocrystals leads to greatly improved operation durability for electrocatalytic ethanol oxidation in alkaline solution, *Adv. Mater.*, 2017, **29**, 1703057.
14. K. Zhang, Z. Xiong, S. Li, B. Yan, J. Wang and Y. Du, Cu₃P/RGO promoted Pd catalysts for alcohol electro-oxidation, *J. Alloys Compd.*, 2017, **706**, 89-96.

15. Y. Chen, Z. Fan, Z. Luo, X. Liu, Z. Lai, B. Li, Y. Zong, L. Gu and H. Zhang, High-yield synthesis of crystal-phase-heterostructured 4H/fcc Au@Pd core-shell nanorods for electrocatalytic ethanol oxidation, *Adv. Mater.*, 2017, **29**, 1701331.
16. Q. Zhang, F. Zhang, X. Ma, Y. Zheng and S. Hou, Facile synthesis of PdS_x/C porous nanospheres and their applications for ethanol oxidation reaction, *J. Power Sources*, 2016, **336**, 1-7.
17. J. Xue, G. Han, W. Ye, Y. Sang, H. Li, P. Guo and X. S. Zhao, Structural regulation of PdCu₂ nanoparticles and their electrocatalytic performance for ethanol oxidation, *ACS Appl. Mater. Interfaces*, 2016, **8**, 34497-34505.
18. M. Wang, R. Ding, Y. Xiao, H. Wang, L. Wang, C.-M. Chen, Y. Mu, G.-P. Wu and B. Lv, CoP/RGO-Pd hybrids with heterointerfaces as highly active catalysts for ethanol electrooxidation, *ACS Appl. Mater. Interfaces*, 2020, **12**, 28903-28914.
19. F. Lv, W. Zhang, M. Sun, F. Lin, T. Wu, P. Zhou, W. Yang, P. Gao, B. Huang and S. Guo, Au clusters on Pd nanosheets selectively switch the pathway of ethanol electrooxidation: amorphous/crystalline interface matters, *Adv. Energy Mater.*, 2021, **11**, 2100187.
20. S. Zhang, A. Pei, G. Li, L. Zhu, G. Li, F. Wu, S. Lin, W. Chen, B. H. Chen and R. Luque, Pd/CuO–Ni(OH)₂/C as a highly efficient and stable catalyst for the electrocatalytic oxidation of ethanol, *Green Chem.*, 2022, **24**, 2438-2450.
21. X. Yang, Z. Liang, S. Chen, M. Ma, Q. Wang, X. Tong, Q. Zhang, J. Ye, L. Gu and N. Yang, A phosphorus-doped Ag@Pd catalyst for enhanced C-C bond cleavage during ethanol electrooxidation, *Small*, 2020, **16**, e2004727.
22. L. Zhang, Q. Chang, H. Chen and M. Shao, Recent advances in palladium-based electrocatalysts for fuel cell reactions and hydrogen evolution reaction, *Nano Energy*, 2016, **29**, 198-219.